applied optics

Optical system design of an atmospheric detector with nadir view and omnidirectional limb view

Xiaoheng Wang[1,2] and Qingsheng Xue[1,*]

[1]Changchun Institute of Optics, Fine Mechanics and Physics, Chinese Academy of Sciences, Changchun 130033, China
[2]University of Chinese Academy of Sciences, Beijing 100049, China
*Corresponding author: qshxue2006@163.com

Received 30 June 2017; revised 18 August 2017; accepted 19 August 2017; posted 21 August 2017 (Doc. ID 301336); published 8 September 2017

A new type of optical system for atmospheric detection is designed by using the principle of panoramic imaging. Compared to the traditional ones, this optical system can observe nadir view and omnidirectional limb view at the same time, thus improving the efficiency and accuracy of the observation data inversion. The optical system consists of a front lens group, a panoramic annular lens, a relay lens group, and a narrowband filter. The nadir view and limb view are shared with the panoramic annular lens and the relay lens group. The narrowband filter is employed to select the specific band and restrain the stray light outside the band. This detector can monitor atmosphere conditions in the nadir field of view of 10° and the limb field of view of 360° × (70.9°–73.3°). Based on this optical design, we develop a prototype for the detector and use it for the field test. The results of experiments verify the feasibility of the optical system design.

OCIS codes: (010.0280) Remote sensing and sensors; (080.2740) Geometric optical design; (220.3620) Lens system design.

https://doi.org/10.1364/AO.56.007454

1. INTRODUCTION

As an important part of space environment, the atmosphere plays a crucial role in human survival and development. Atmospheric monitoring helps us understand overall atmospheric behaviors, study climate phenomenon, and prevent air pollution, etc. In the atmosphere, electromagnetic radiation is the main form of energy transfer. As shown in Fig. 1, different atmospheric components have different scattering and absorption characteristics over the solar band. Therefore, remote sensors are used to observe the radiation transmitted in the atmosphere. By analyzing the detection data, one can understand the composition and the change of the atmosphere [1,2].

There are three detection modes for traditional atmospheric detection instruments: the nadir mode, the occultation mode, and the limb mode [3–5]. As shown in Fig. 2, the nadir mode detects the backward scattered light from the zenith, the occultation mode detects the transmitted light in the horizontal direction as the sun rises or sets, and the limb mode detects the scattered light in the horizontal direction. The three detection methods each have their own characteristics: the nadir mode is suitable for detection of the overall distribution of air composition, and the occultation and limb modes for detection of the variation of atmospheric conditions at different altitudes. It is desirable to get the total amount and the vertical profile of the atmosphere simultaneously, which requires that the optical system of the atmospheric detector has both the nadir detection and the limb or occultation detection. Compared to the occultation mode, the limb detection is not limited by the detection period and has higher detection efficiency. Thus, we select the nadir and the limb modes for the optical atmospheric detector.

However, the traditional limb mode can only detect a narrow band of area in a certain direction [6,7], so the coverage is small and the observation data are insufficient and not cross-correlate. The catadioptric panoramic imaging system is a new type of secondary imaging system with negative focal length, which utilizes a panoramic annular lens (PAL) to image within 360° directions [8–11]. Therefore, we can use the panoramic imaging technology to detect the limb of atmosphere in all directions. First, the beam of the limb field of view enters the PAL, and it is imaged inside the PAL after the first reflection. And then, the image is passed through the residual catadioptric surfaces of the optical system and imaged on the focal plane. However, the catadioptric panoramic imaging technique has the characteristic that there is an observation blind spot in front of the optical system, so the traditional catadioptric panoramic imaging technology cannot detect the nadir field of view. Bai and others proposed the use of dichroic optical elements to eliminate the central blind spot in front of the optical system (the dichroic elements are used to transmit visible light and reflect ultraviolet light, and the ultraviolet light is imaged on the PAL imaging area while the visible light is imaged on the blind area of a conventional PAL) [12].

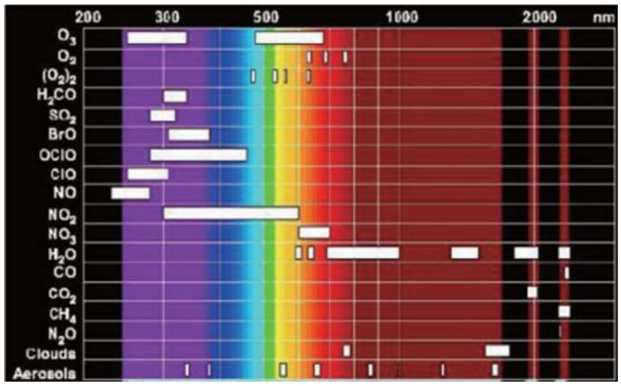

Fig. 1. Absorption wave bands of different atmospheric components.

Taking into account the future inversion of detection data, the nadir and limb fields of view must have the same spectral range, so we cannot use the dichroic filter. We use the method of coating in a specific area of the PAL to control its catadioptric properties for different fields of view, and to realize the simultaneous detections of the nadir field of view and omnidirectional limb field of view (Fig. 3).

2. OPTICAL SPECIFICATION

Figure 4 shows a schematic of the detection observation of the instrument. The detector is mounted on a low-orbit satellite at the altitude of 400 km (H_1), of which the width coverage L_1 of the nadir detection is 70 km. Therefore, the nadir field of view α is determined by

$$\alpha = 2\arctan\left(\frac{L_1/2}{H_1}\right) = 10°. \quad (1)$$

The distance H_2 from the instrument to the limb observation point is 2150 km, the detection height range of the limb field of view is 10–90 km, and the width coverage L_2 in the limb altitude direction is 80 km. The view angle β in the limb height detection is

$$\beta = 2\arctan\left(\frac{L_2/2}{H_2}\right) = 2.13°. \quad (2)$$

We choose β as 2.4° in order to have abundant detecting allowance, so the limb observation field of view is 360° × (70.9°–73.3°).

We require the spatial resolution L of the nadir field of view is less than 1.2 km, and that of the limb field of view is less than 6 km. The optical system focal length is given by

$$|f'| = \frac{a \cdot H}{L}, \quad (3)$$

where a is the size of the CCD pixel, and H is the detection distance. The CCD 47-20 produced by E2V with a pixel size of 13 μm × 13 μm is used as the detector of this system. It can be calculated that the nadir viewing focal length f_1 is 4.33 mm and the limb viewing focal length f_2 is –4.66 mm. We choose 5 mm as the absolute value of the focal length of the two fields of view. The specifications of this optical system are shown in Table 1.

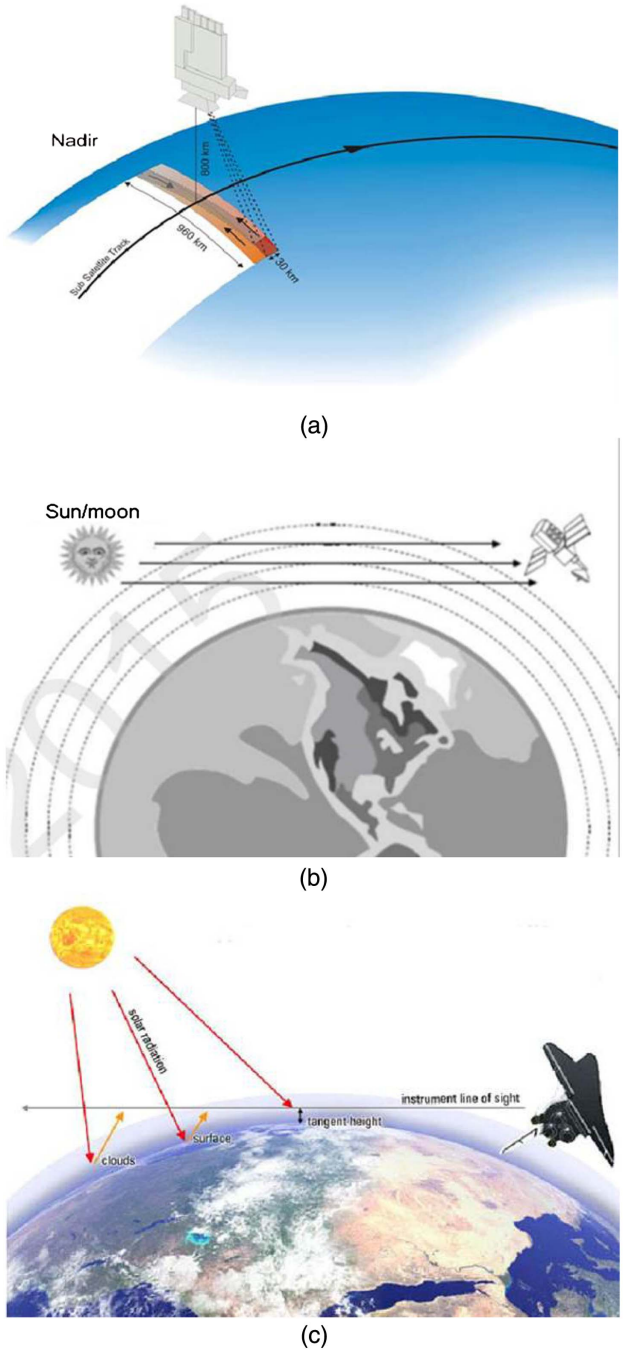

Fig. 2. Atmospheric detection modes. (a) The nadir mode, (b) the occultation mode, (c) the limb mode.

3. IMAGE-PLANE ILLUMINATION ANALYSIS

It is required that the relative illumination of our optical system reach 90% or more for all fields of view. However, the image-plane illumination decreases as the field of view increases, and the limb half field of view of this detector is already 73.3°. Therefore, it is necessary to determine the relation between the image-plane illumination and the field of view, so that one can take effective measures to solve the problem of illumination uniformity.

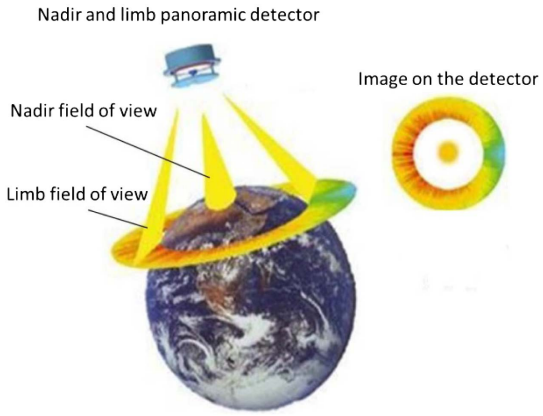

Fig. 3. Detecting mode of the nadir view field and omnidirectional limb view field.

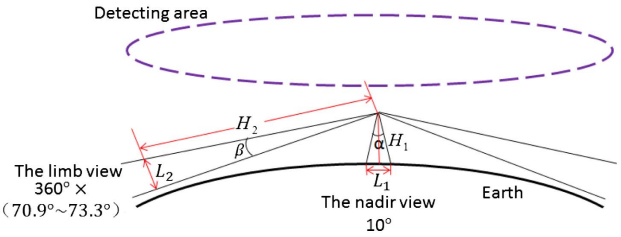

Fig. 4. Aerial observation schematic of the detector.

Table 1. Optical Specifications of the Imaging System

Parameters	Nadir View Configuration	Limb View Configuration
F-number	3.5	3.5
Focal length	5 mm	−5 mm
FOV	10°	360° × (70.9°–73.3°)
Central wavelength	265 nm 295 nm 360 nm 540 nm 602 nm 664 nm	265 nm 295 nm 360 nm 540 nm 602 nm 664 nm
Bandwidth	40 nm	40 nm
MTF	≥0.5 at 50 lp/mm	≥0.5 at 38.5 lp/mm
Relative illumination	≥90%	≥90%

Figure 5 shows the transfer relation between the object and the image. Here ds is a tiny element of area in the object plane, which is projected into ds' in the image plane by the optical system. The distance from the entrance pupil to the object plane is R, the effective light passing area of the object center O is S_e, and the solid angle subtended at O by the entrance pupil is Ω_0. For an off-axis area element, the distance from the center of entrance pupil to ds is $R/\cos\omega$, the effective light passing area of ds is $S_e \cdot \cos\omega$, and the solid angle Ω subtended at ds by the entrance pupil is

$$\Omega = \frac{S_e \cos\omega}{(R/\cos\omega)^2} = \Omega_0 \cos^3\omega. \tag{4}$$

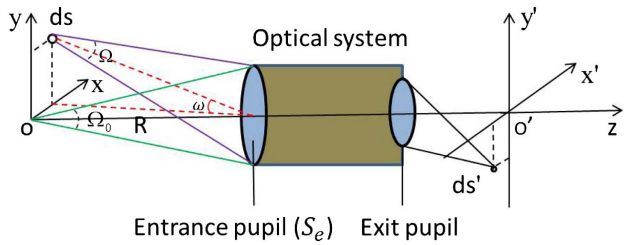

Fig. 5. Transfer relation between the object and image.

At the center of the entrance pupil, the luminous intensity from the area element ds is

$$I = L\cos\omega ds, \tag{5}$$

where L is the radiance brightness of the object. Thus the radiation flux $\varnothing$ received by entrance pupil is

$$\Phi = I \cdot \Omega = L\Omega_0 \cos^4\omega ds. \tag{6}$$

Let the optical system transmittance be τ, and the image-plane illumination E' can be obtained as

$$E' = \frac{\Phi \cdot \tau}{ds'}. \tag{7}$$

Combining Eqs. (6) and (7) gives

$$E' = \tau L\Omega_0 \cos^4\omega \frac{ds}{ds'}. \tag{8}$$

ds/ds' can be replaced by $1/\beta^2$, and β is the lateral magnification of the optical system. Thus, Eq. (8) can be rewritten as

$$E' = \tau L\Omega_0 \frac{\cos^4\omega}{\beta^2}. \tag{9}$$

Equations (8) and (9) show that the image illumination decreases as the fourth power of the cosine of the half field of view. So the image-plane illumination of the edge field of view is much lower than that of the paraxial field of view, and we must take appropriate measures to improve the image-plane illumination of the large field of view.

The limb field of view of the optical system uses the $f-\theta$ projection relation. It is easy to calibrate the relationship between the image point position and the field once the distortion curve is given. It can be seen from Eq. (9) that, with the increase of the half field of view (i.e., decrease of $\cos\omega$), one has to reduce the lateral magnification β in order to prevent the decline of image-plane illumination. Barrel distortion could make the magnification of the large field of view less than that of the small field of view, so the image formed by the object of the large field of view can be compressed by use of barrel distortion, and the decline of image-plane illumination can be reduced.

The half field of view of the optical system is as large as 73.3°, and the requirements for uniformity of the image plane are stringent. The use of barrel distortion alone cannot meet these requirements, so we need to find other ways to further improve the illumination at the edge of the field of view. It can be seen from Eq. (8) that, as the value of $\cos\omega$ is decreasing, we can increase ds and decrease ds' to ensure the illumination is stable, which can be achieved by changing

the aperture aberrations. Thus, we improve the image-plane illumination with barrel distortion and aperture aberrations.

4. OPTICAL SYSTEM DESIGN AND OPTIMIZATION

A. General Design Scheme

The optical structure of the atmospheric detector is shown in Fig. 6, which consists of a former lens group (FLG), a PAL, a relay lens group (RLG), and a narrowband filter. For the limb field of view, the main function of the PAL is to obtain the large field of view at an appropriate angular magnification. The function of the RLG is to transfer the image to the CCD detector. The light from the limb field of view refracts into the PAL, undergoes two reflections inside, and refracts out of the PAL. Then the RLG passes the beam from the PAL to the focal plane at an appropriate magnification. Since the PAL has a symmetric structure, it is possible to detect the atmosphere in the limb 360° direction. For the nadir field of view, the light first passes through the FLG to compress the diameter, and subsequently through the central area of the PAL into the RLG. Finally, the RLG passes the beam to the focal plane. For the nadir field of view, the two surfaces of the PAL are transmissive (and not reflective), so the PAL can be regarded as a thick lens. A narrowband filter is placed between the RLG and the focal plane for band selection and out-of-band stray light suppression. In addition, the instrument is designed for the spatial application and it must have the ability to resist radiation. Thus, the first two lenses of the FLG and the PAL use anti-radiation fused silica material.

B. Panoramic Annular Lens Design

The PAL has different effects on the light from the two fields of view, and thus plays an important role in the image quality of the optical system. The PAL is required to image within the field of view of 360° × (70.9°–73.3°), and the field curvature is an important parameter to measure the image quality for large field of view. The field curvature is determined by the Petzval sum P, and in order to achieve good image quality, the Petzval sum must be zero, which is

$$P = \sum_{i=1}^{m} P_i = 0. \tag{10}$$

In general, the P_i of the RLG is positive, so the P_i of the PAL must be negative [13]. The P of the optical system can be estimated as

$$P = \sum_{i=1}^{m} P_i = J^2 \sum_{i=1}^{m} \frac{n_i' - n_i}{n_i' n_i} c_i, \tag{11}$$

where J is the Lagrange invariant, n_i and n_i' are the refractive indices before and after the i-th surface, respectively, and c_i is the curvature of the i-th surfaces. For the reflective surface, n_i' is equal to $-n_i$.

A more detailed structure of the PAL is shown in Fig. 7, which is composed of two reflection surfaces [Figs. 7(d) and 7(e)] and three transmission surfaces [Figs. 7(f)–7(h)]. To facilitate the processing of the PAL, we set the surfaces d and h to be of the same curvature, and surfaces g and e to be planar, which serve as reference for the other surfaces. We change the catadioptric properties of the PAL surfaces by coating different films on different areas.

For the limb field of view, the light passes through the transmission surface f into the PAL, then is reflected twice by the reflection surfaces d and e, and finally passes through the transmission surface h out of the PAL. By Eq. (11) we can obtain the Petzval coefficient P_1 of the limb beam caused by the PAL:

$$P_1 = J^2 \left[\frac{n_p - 1}{n_p} c_1 + 2\frac{c_2}{n_p} + \frac{1 - n_p}{n_p} c_2 \right], \tag{12}$$

where n_p is the refractive index of the PAL, c_1 is the curvature of the surface f, and c_2 is the curvature of surfaces d and h. One needs to choose appropriate curvature to ensure that $P_1 < 0$.

For the nadir field of view, the light enters the PAL from transmission surface g, and passes through surface h out of the PAL. The Petzval coefficient P_2 of the nadir beam caused by the PAL is

$$P_2 = J^2 \frac{1 - n_p}{n_p} c_2. \tag{13}$$

It can be seen from this equation that P_2 is always greater than zero.

We further note that all the surfaces of the PAL are spherical, which has the advantages of easy processing and low cost.

C. Limb Detection Structure

In general, the optical system has two kinds of projection: tangent projection and equidistant projection. And their relationship is shown in Eqs. (14) and (15), respectively:

$$y' = f' \cdot \theta, \tag{14}$$

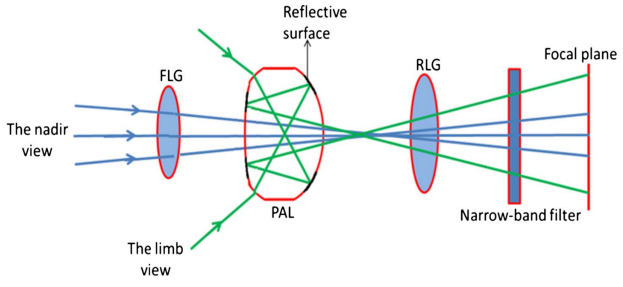

Fig. 6. Optical structure of the atmospheric detector.

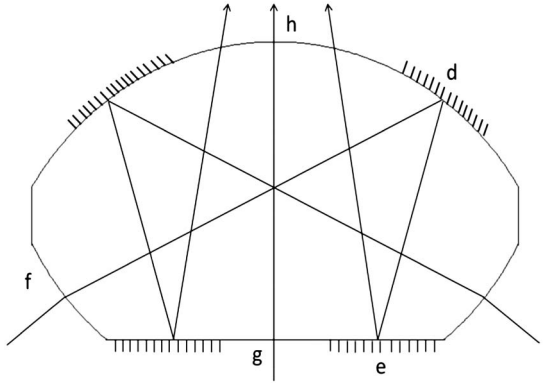

Fig. 7. Panoramic annular lens (PAL).

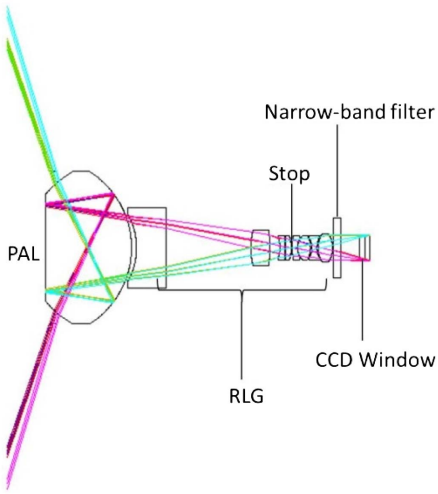

Fig. 8. Limb detecting structure.

$$y' = f' \cdot \tan\theta, \tag{15}$$

where y' is the ideal image height, f' is the focal length, and θ is the half field of view of the optical system. The area between the nadir field of view and the limb field of view is not required to be imaged, but this area also occupies a certain area on the CCD detector. The limb half field of view of this optical system is (70.9°–73.3°). It can be seen from Eqs. (8) and (9) that the image height of the tangent projection is about 3 times than that of equidistant projection, and it will cause a great waste of CCD. Therefore, the limb view structure uses the equidistant projection mode.

In the optical system, the RLG is responsible for image transfer and aberration correction, and has the characteristics of large relative aperture and medium field of view. Therefore the RLG is crucial to the entire system design. We use the complex three-piece structure as the initial structure of the RLG, and place a narrowband filter behind the RLG for band selection and stray light suppression. The RLG is composed of eight single lenses. The material of positive lenses and negative lenses are CaF_2 and fused silica, respectively. The stop is placed between the fourth and the fifth lenses of the RLG. The focal length of the RLG is 16.5 mm and the magnification is 1.15. We connect the PAL and the RLG under the pupil-matching condition, and optimize the whole system. In the optimization, the RLG is optimized first, and the PAL is further optimized under the condition of any light does not overflow from the RLG. After that, the PAL and the RLG are optimized as a whole to get a better image quality. The structure of this design is shown in Fig. 8.

D. Nadir Detection Structure

We have known from Eq. (13) that the Petzval coefficient of the nadir beam caused by the PAL is always greater than zero. So we need to add the FLG in front of the PAL to correct the field curvature. The FLG consists of two positive lenses and two negative lenses that can correct the field curvature while compressing the diameter of the beam of the nadir field of view.

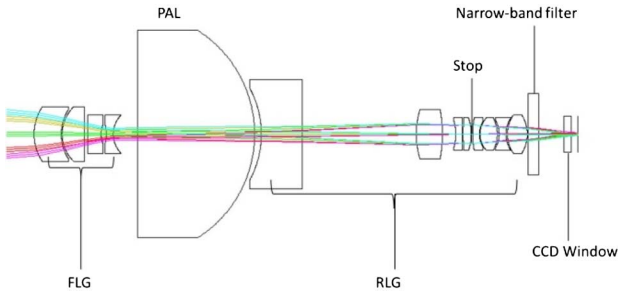

Fig. 9. Nadir detecting structure.

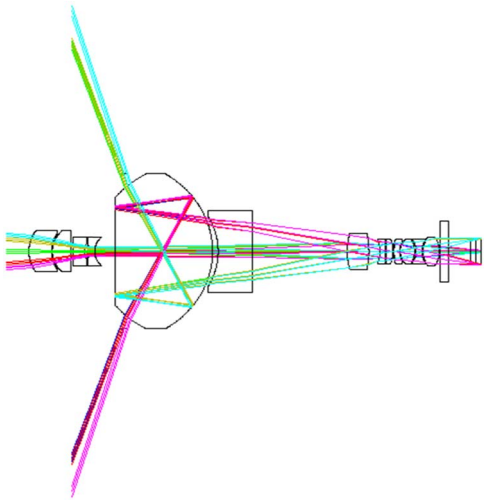

Fig. 10. Nadir and omnidirectional limb detection structure.

In the design, one has to ensure that the exit pupil of the FLG matches the entrance pupil of the back of the group.

It must also be ensured that the PAL and RLG structure do not change, and only the FLG is optimized. The design result is shown in Fig. 9.

E. Overall Optical System of the Detector

We used the multi-configuration function of ZEMAX to combine the nadir structure and the limb structure, and optimized the two configurations at the same time to achieve good image quality for both fields. The optimized system is shown in Fig. 10, which can observe the nadir field of view and the omnidirectional limb field of view simultaneously.

5. IMAGE PERFORMANCE AND TOLERANCE ANALYSIS

A. Image Performance

We establish the model of the optical system in the LIGHTTOOLS software for imaging simulation. We can get the ray tracing map (Fig. 11) and the distribution of the image on the focal plane (Fig. 12). The image of the nadir field of view is a bright spot, and that of the limb field of view is an annular pattern. The simulated picture is consistent with the expected result, and thus the design is reasonable.

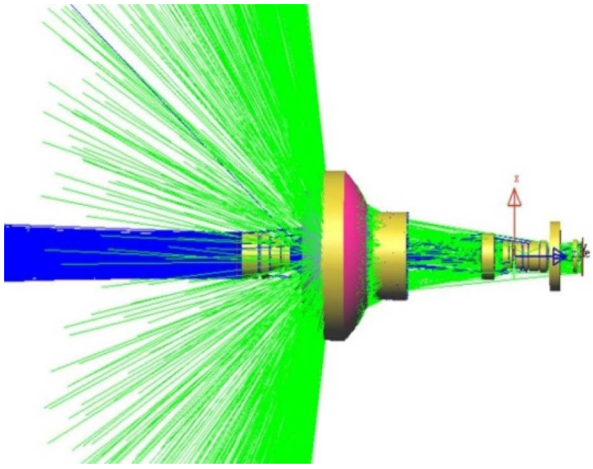

Fig. 11. Ray tracing map.

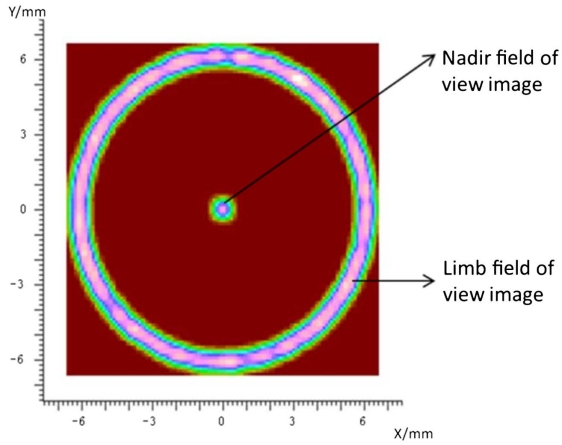

Fig. 12. Distribution of the image on the focal plane.

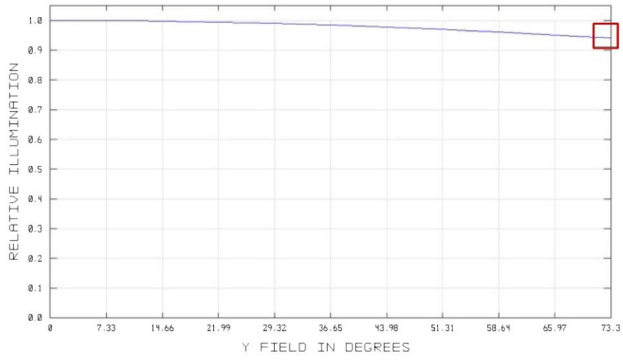

Fig. 13. Relative illumination of the image plane.

From Eqs. (8) and (9), we have known that the image illumination decreases with the fourth power of the cosine of the half field of view. The optical system has a large field of view and high illumination uniformity requirements. As described in Section 3, we employ the barrel distortion and the aperture aberrations to improve the illumination of the edge field. The relative illumination is shown in Fig. 13. However, the

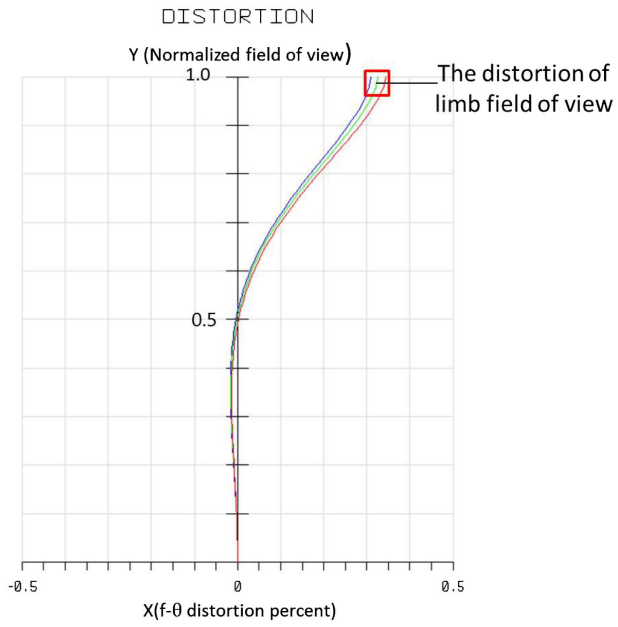

Fig. 14. $F-\theta$ distortion.

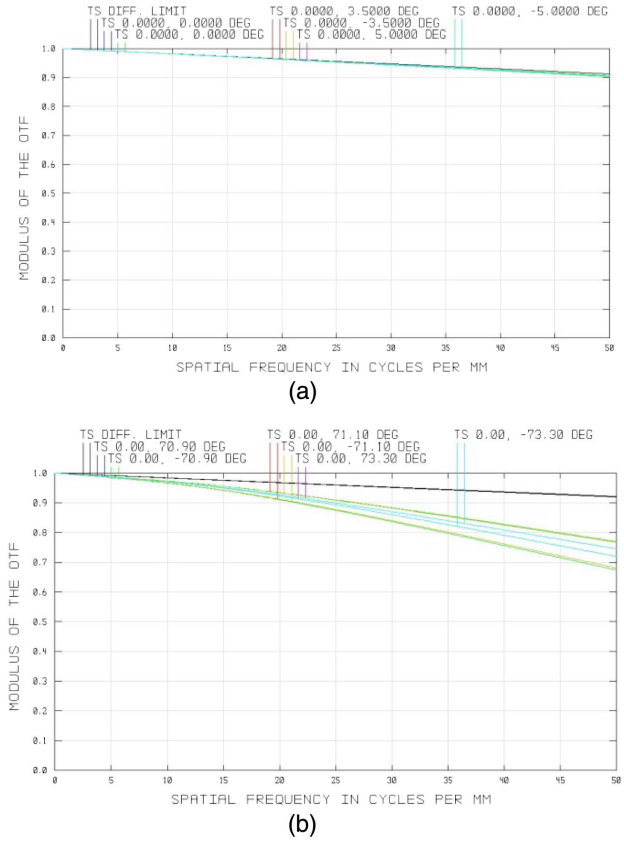

Fig. 15. MTFs of optical system. (a) MTF of the nadir field of view, (b) MTF of the limb field of view. The Nyquist frequency of the CCD detector is 38.5 lp/mm.

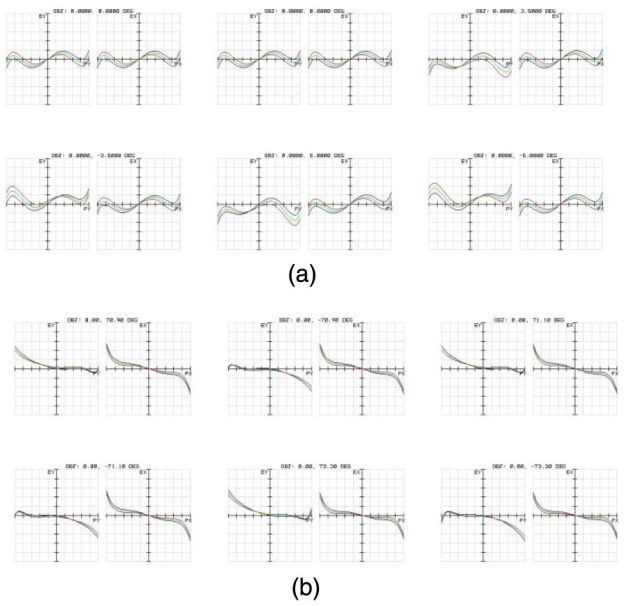

Fig. 16. Ray fans of the optical system. (a) Ray fans of the nadir field of view, (b) ray fans of the limb field of view.

optical system only detects the area of the limb field of view resulting in the illumination curve is meaningful just in the part surrounded by the red frame in Fig. 13. It can be seen that the relative illumination of the limb field of view on the image is greater than 94%, better than the design indicator.

As described in Section 4.C, the optical system of limb observation adopts the equidistant projection relationship. The $F-\theta$ distortion of this optical system is given by

$$f-\theta\,\text{distortion} = \frac{y'-y}{y}\cdot 100\%, \tag{16}$$

where y' is the real image height. The $F-\theta$ distortion of the system is shown in Fig. 14, and it is meaningful just in the limb field of view. It can be seen from Fig. 14 that the $F-\theta$ distortion of the optical system is about 0.35% and the distortion correction is better.

The modulation transform function (MTF) reflects the image quality of the optical system. As shown in Fig. 15(a), the MTF of the nadir field of view is greater than 0.9 at 50 lp/mm, better than 0.5 at 50 lp/mm of the design indicators. The MTF of the limb field of view is shown in Fig. 15(b), which is greater than 0.75 at 50 lp/mm, better than 0.5 at 38.5 lp/mm of the design indicators.

Ray fans can visually display the various aberrations of the optical system. Figures 16(a) and 16(b) are the ray fans of the nadir and limb fields of view, respectively. The maximum corresponding coordinate scales of ray fans are 5 μm and 20 μm, respectively.

B. Tolerance Analysis

The rational tolerances are necessary for the fabrication of the optical system. The predetermined tolerances of the system are shown in Table 2. According to the analysis of the tolerance simulation results, the mean MTFs of the nadir and limb detection structures are 0.81 at 50 lp/mm and 0.61 at 50 lp/mm, which are 0.10 and 0.13 less than nominal values, respectively. The result meets the imaging requirements of the optical system.

Table 2. Tabulation of Precision Optical Fabrication Tolerances

Tolerance Items	Value
Radius (fringes)	1
Thickness (mm)	0.015
Decenter X/Y (mm)	0.015
Tilt X/Y (degrees)	0.0083
S + A irregularity (fringes)	0.2
Index of refraction	0.0001
Abbe number (%)	1

6. EXPERIMENTAL PROTOTYPE AND ITS PICTURES

In order to further verify the feasibility of this design, we developed an experimental prototype of the atmospheric detector. As shown in Fig. 17, the mechanical structure consists of several lens holders and a lens cone. The bench center is used to ensure the assembly error is not out of the tolerance range. The prototype is shown in Fig. 18.

We used the experimental prototype for the field test, and its pictures are shown in Fig. 19, where Fig. 19(a) is the total image, and Figs. 19(b) and 19(c) are the enlarged pictures of

Fig. 17. Lens bases and lens cone of the prototype.

Fig. 18. Experimental prototype of the atmospheric detector.

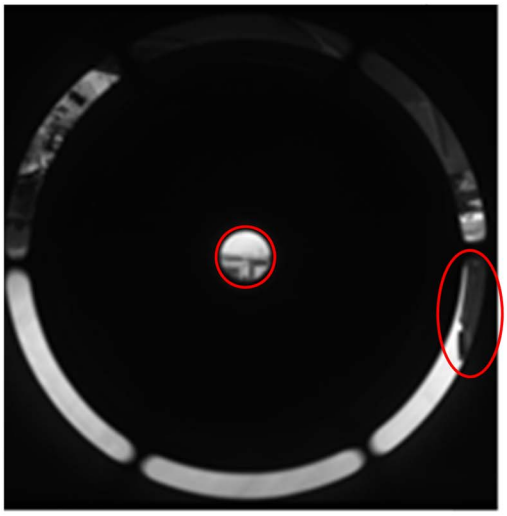

(a)

(b)

(c)

Fig. 19. Image taken by the experimental prototype. (a) Total picture, (b) picture of the nadir field of view. The beam of the nadir field of view is imaged on the CCD detector in the form of a central circular spot. And the circular spot is only about 68 pixels across the diameter across the optical specification. Therefore, the picture of the nadir field of view is blurred after amplification. (c) Picture of the limb field of view.

the areas surrounded by the red coils in Fig. 19(a). It is possible to recognize the buildings in the image of the nadir and the limb fields of view and proves the feasibility of our design.

7. CONCLUSION

We have designed an optical system for atmospheric detection. Compared to the conventional remote sensing detector with single detection mode, this system can simultaneously observe at the nadir field of view of 10° and the limb field of view of 360° × (70.9°–73.3°). We can use the collected data by this optical system to retrieve the total amount and the vertical profile of the atmosphere. The limb observation has the characteristic of omnidirectional field of view, which provides more comprehensive data than the traditional single field of view limb observation, and the inversion accuracy can be improved by cross comparison between the data in adjacent observation directions. The design of this optical system provides a novel idea for future spatial atmospheric remote sensors.

Funding. National Natural Science Foundation of China (NSFC) (41575023); National Key Research and Development Plan (2016YFB0500300, 2016YFB0500301); Jilin Scientific and Technological Development Program (20160520096JH).

REFERENCES

1. K. N. Lion, *An Introduction to Atmospheric Radiation*, 2nd ed. (Academic, 2002).
2. G. L. Stephens, *Remote Sensing of the Lower Atmosphere* (Oxford University, 1994).
3. S. Noël, H. Bovensmann, M. W. Wuttke, J. P. Burrows, M. Gottwald, E. Krieg, A. P. H. Goede, and C. Muler, "Nadir, limb, and occultation measurements with SCIAMACHY," Adv. Space. Res. **29**, 1819–1824 (2002).
4. H. G. Werij, C. Olij, A. E. Zoutman, and A. Kamp, "SCIAMACHY: the completion of a new-generation instrument for studying the atmosphere," Proc. SPIE **2957**, 20–30 (1997).
5. S. B. Chen, "A new technique for atmospheric chemistry observations," Proc. SPIE **6031**, 60310R (2006).
6. R. D. Mcpeters, S. J. Janz, E. Hilsenrath, T. L. Brown, D. E. Flittner, and D. F. Heath, "The retrieval of O_3 profiles from limb scatter measurements: results from the shuttle ozone limb sounding experiment," Geophys. Res. Lett. **27**, 2597–2600 (2000).
7. D. E. Flittner, E. Hilsenrath, S. J. Janz, R. P. Loughman, R. D. McPeters, and D. F. Rault, "Retrievals from the limb ozone retrieval experiment on STS107," Proc. SPIE **5542**, 215–226 (2004).
8. Z. Huang, J. Bai, and X. Y. Hou, "Design of panoramic stereo imaging with single optical system," Opt. Express **20**, 6085–6096 (2012).
9. J. H. Wang, Y. C. Liang, and M. Xu, "Design of panoramic lens based on ogive and aspheric surface," Opt. Express **23**, 19489–19499 (2015).
10. G. L. Kweon, K. T. Kim, G. H. Kim, and H. S. Kim, "Folded catadioptric panoramic lens with an equidistance projection scheme," Appl. Opt. **44**, 2759–2767 (2005).
11. T. Ma, J. C. Yu, P. Liang, and C. H. Wang, "Design of a freeform varifocal panoramic optical system with specified annular center of field of view," Opt. Express **19**, 3843–3853 (2011).
12. L. J. Luo, J. Bai, X. D. Zhou, Q. Liu, and Y. Yao, "Non-blind area PAL system design based on dichroic filter," Opt. Express **24**, 4913–4923 (2016).
13. X. D. Zhou, J. Bai, C. Wang, X. Y. Hou, and K. W. Wang, "Comparison of two panoramic front unit arrangements in design of a super wide angle panoramic annular lens," Appl. Opt. **55**, 3219–3225 (2016).